

Mechanism of CDK activation revealed by the structure of a cyclinA-CDK2 complex

Philip D. Jeffrey^{*}, Allcia A. Russo^{*}, Kornelia Polyak[†], Emma Gibbs[†], Jerard Hurwitz[‡], Joan Massagué[†] & Nikola P. Pavletich^{*}

^{*} Cellular Biochemistry and Biophysics Program, [†] Cell Biology and Genetics Program and the Howard Hughes Medical Institute, [‡] Molecular Biology Program, Memorial Sloan-Kettering Cancer Center, New York, New York 10021, USA

The crystal structure of the human cyclinA-cyclin-dependent kinase2 (CDK2)-ATP complex has been determined at 2.3 Å resolution. CyclinA binds to one side of CDK2's catalytic cleft, inducing large conformational changes in its PSTAIRE helix and T-loop. These changes activate the kinase by realigning active site residues and relieving the steric blockade at the entrance of the catalytic cleft.

THE eukaryotic cell cycle is coordinated by several related Ser/Thr protein kinases, each consisting of a catalytic cyclin-dependent kinase (CDK) subunit and a regulatory cyclin subunit (reviewed in refs 1, 2). The transient appearance of these cyclin-CDK complexes drives cell cycle events such as cell growth³ (cyclinD-CDK4 and cyclinD-CDK6 in G1), DNA replication^{4,5} (cyclinE-CDK2 in G1/S and cyclinA-CDK2 in S) and cell division⁶ (cyclinA-CDK1 and cyclinB-CDK1 in G2 and M).

The CDK subunit is inactive as a protein kinase without the cyclin subunit⁷. The binding of the cyclin subunit confers basal kinase activity to the complex⁸, and phosphorylation of a threonine residue in the CDK subunit by CDK-activating kinase⁷ (CAK) results in full activity. Recent studies indicate that binding of the cyclin subunit also modulates the substrate specificity of the kinase⁹. Substrates include the retinoblastoma protein, Rb, which is preferentially associated with cyclinD-CDK4 complexes¹⁰; p107 (ref. 11), E2F (ref. 12), and replication protein-A (ref. 13), which are phosphorylated by cyclinA-CDK2; and histone H1, which is phosphorylated by cyclinB-CDK1 (refs 13, 14).

Cyclins, which vary in relative molecular mass (M_r) from 30K to 45K, share a homologous region of about 100 amino acids (30–50% similarity among cyclins A, B, D1 and E) termed the cyclin box¹⁵. CDKs are highly homologous⁹ (40–75% similarity among CDK1 through CDK7) and contain a conserved catalytic core of approximately 300 amino acids common to all eukaryotic protein kinases¹⁶. Crystallographic studies of several eukaryotic protein kinases^{17–20}, including CDK2 (ref. 21) and the cyclic AMP-dependent protein kinase catalytic subunit (PKA)²², have shown that they all share the same fold and tertiary structure. When these structures are compared in detail, however, significant differences in their catalytic sites become evident, which are thought to reflect differences in their regulation. Whereas CDKs are activated by the binding of their regulatory cyclin subunit, for example, PKA is active in the free form and the binding of its regulatory subunit is inhibitory²².

To understand how cyclins activate CDKs, we have determined the crystal structure of a human cyclinA-CDK2-ATP complex at 2.3 Å resolution and refined it to a crystallographic *R*-factor of 20.8%. Comparison of the CDK2 structure in this complex with that of catalytically inactive free CDK2 (ref. 21) reveals that cyclin binding causes large conformational changes in CDK2's active site which we propose are responsible for activating CDKs.

Structure determination

Because human cyclinA aggregates at high concentrations, we used limited proteolytic digestion to identify a 29K structural

domain more amenable to crystallization (residues 173–432). This fragment, which contains core sequences common to members of the cyclin family, has CDK2 binding and activating properties identical to those of full-length cyclinA. The histone H1 phosphorylation activity of the CDK2-cyclinA fragment complex is 0.30 pmol phosphate transferred per min per pmol CDK2, compared to 0.28 for the CDK2-full-length cyclinA complex. Addition of a CDK-activating kinase preparation increases the activities to 5.1 and 4.8 pmol phosphate, respectively. Similar results have been obtained with truncated *Xenopus laevis* cyclinA fragments analogous to the one reported here^{23,24}. Both complexes are inhibited to the same extent by the p27^{Kip1} CDK inhibitor protein²⁵ (0.024 residual activity), and both cyclinA molecules have similar *in vivo* mitotic activity when synthesized in *Xenopus laevis* oocytes from microinjected capped complementary RNA²⁴.

The cyclinA fragment-CDK2-ATP complex produced three crystal forms from similar crystallization conditions (Table 1). An orthorhombic form in spacegroup $P2_12_12_1$ with $a=132.9$, $b=149.3$, $c=73.7$ Å grew readily; a hexagonal form in spacegroup $P6_222$ with $a=b=185.1$, $c=214.4$ Å grew infrequently; and a third form grew twinned and was not characterized. Both characterized forms contain two complexes in the asymmetric unit and have similar non-crystallographic symmetry (approximate two-fold symmetry). The structure of the complex in the orthorhombic crystals was determined by multiple isomorphous replacement (Table 1), and the structure of the complex in the hexagonal form was determined by molecular replacement using the partially refined orthorhombic form structure (Table 1). The structures in the two forms are essentially identical, and here we consider the hexagonal form, which has been refined at 2.3 Å resolution. The current model of the asymmetric unit contains 2 cyclinA molecules (residues 173–432), 2 CDK2 molecules (residues 1–298), 2 ATP molecules and 416 water molecules. The structure (Fig. 1) has an *R*-factor of 20.8% for data from 6.0 to 2.3 Å, with 0.013 Å r.m.s. deviation from ideal bond lengths and 1.77° r.m.s. deviation from ideal bond angles.

Overall structure of the complex

The structure of CDK2 consists of an amino-terminal lobe (residues 1–85) rich in β -sheet and a larger, mostly α -helical, carboxy-terminal lobe. ATP binds in a deep cleft between the two lobes which contains catalytic residues conserved among eukaryotic protein kinases and is presumed to be the site of protein substrate binding and catalysis. CyclinA has two helical domains with identical chain topology. It binds to one side of the catalytic cleft, interacting with both lobes of CDK2 to form a large, continuous protein-protein interface (Fig. 2a, b)

TABLE 1 Diffraction data, MIR analysis and refinement statistics

Data set	Resolution (Å)	Reflections		Data coverage (%)	R_{sym} (%)	MIR analysis (20–3.2 Å)		
		Measured	Unique			Sites	MFID (%)†	Phasing power‡
Native 2 ($P6_222$)	2.3	677,413	86,466	90.2	6.1			
Native-Mg ($P2_12_12_1$)	2.5	174,498	47,667	92.3	6.5			
Native 1 ($P2_12_12_1$)	3.1	81,900	26,362	96.3	4.6			
HgCl ₂	3.2	63,110	23,344	93.3	4.4	2	0.12	2.56
Thimerosal	3.4	35,140	20,928	78.8	5.9	5	0.17	1.31
UO ₂ (OAc) ₂	3.2	75,102	24,218	96.0	5.9	2	0.16	1.62
Sm(OAc) ₃	3.4	41,907	17,685	85.1	6.6	2	0.12	0.43
K ₂ Au(CN) ₄	3.8	31,511	13,104	86.7	7.4	6	0.11	0.81
						r.m.s.		
Refinement	Resolution (Å)	Reflections (with $ F > 2\sigma$)	Total number of atoms	waters	R-factor (%)§	Bonds (Å)	Angles (°)	B-factor (Å ²)
Hexagonal	6.0–2.3	70,208	9,476	416	20.8	0.013	1.77	3.0
Orthorhombic	7.0–2.5	43,576	9,157	97	22.8	0.013	1.89	2.5

Protein expression and purification. Human cyclinA was expressed in *Escherichia coli* and purified as described⁸. The cyclinA fragment (residues 173–432) was produced by digesting 50 mg cyclinA with 25 µg subtilisin at 4 °C for 90 min, and it was purified by cation exchange chromatography (the identity of the fragment was determined by N-terminal sequencing and by subcloning into *E. coli*). The N-terminal 172 residues absent in the fragment do not have significant homology in other cyclins, and are absent from cyclins D and E¹⁵. Human CDK2 was expressed in insect cells using a baculovirus vector, and was purified as described³⁴. Mass spectroscopy (by the electrospray ionization triple-stage quadrupole method) of the baculovirus-expressed CDK2 preparation indicated that it consisted predominantly of a single species (>95%). The mass was consistent with the unphosphorylated CDK2 molecule having an acetyl group at the N-terminal methionine (Edman degradation negative). The complex was prepared by mixing CDK2 and the cyclinA fragment at an equivalent molar ratio, followed by purification on a gel filtration column and concentration by ultrafiltration to 25 mg ml⁻¹ in a buffer of 40 mM HEPES, 0.2 M NaCl, 5 mM dithiothreitol (DTT), pH 7.0. **Crystallization and data collection.** Crystals were grown at 4 °C by the hanging drop vapour diffusion method. The complex was mixed with an equal volume of the well buffer containing 28% saturated (NH₄)₂(SO₄), 1 M KCl, 40 mM HEPES, 5 mM DTT, pH 7.0, and ATP was added to the drop at a final concentration of 10 mM. Magnesium was not used in the crystallization because it interfered with the growth of large, diffraction-quality crystals. All diffraction data were collected at -170 °C. The Native-1 and derivative data sets were collected using an R-AXISIIIC imaging plate detector mounted on a Rigaku 200HB generator. The Native-2 and Native-Mg data sets were collected using a CCD detector at the A1 beamline of the Cornell High Energy Synchrotron Source (MacChess). For flash freezing, crystals were successively transferred to cryoprotectant buffers that contained increasing amounts of glycerol (10, 20 and 30%), and were then flash frozen in a stream of nitrogen gas at -170 °C in 50% saturated (NH₄)₂(SO₄), 30% glycerol, 50 mM KCl, 5 mM ATP, 100 mM HEPES, pH 7.0. **MIR analysis, model building and refinement.** Heavy-atom soaks were performed using the orthorhombic form crystals in a buffer of 50% saturated (NH₄)₂(SO₄), 0.25 M KCl, 5 mM ATP and 100 mM HEPES, pH 7.0, containing one of the following heavy-atom solutions: 2 mM HgCl₂ for 5 h, 0.6 mM thimerosal for 15 h, 4 mM uranyl acetate for 5 days, 3 mM samarium acetate for 5 h, or 5 mM dipotassium gold cyanide for 13 h. Initial MIR phases were calculated at 3.2 Å resolution with the program PHARE³⁵ and had a mean figure of merit of 0.62. The MIR map was improved by solvent flattening³⁶ and non-crystallographic symmetry (n.c.s.) averaging with the program RAVE³⁷. The initial MIR map and the n.c.s.-averaged map were used to build the initial model with the programs O³⁸ and CHAIN³⁹ (CDK2 was built based on a model derived from the PKA structure). Successive rounds of rebuilding, simulated annealing refinement with the program X-PLOR⁴⁰, and phase combination with the program SIGMA³⁵ allowed complete interpretation of the cyclinA and CDK2 structures in the orthorhombic crystal form. After several cycles of refinement with the full model, X-PLOR omit maps were used to systematically check every part of the complex (about 2–5% of the structure was deleted in each calculation, and simulated annealing was used to reduce model bias in the omit maps). **Molecular replacement solution of the hexagonal form structure.** The structure of the hexagonal form was determined by molecular replacement with the programs MERLOT⁴¹, BRUTE⁴² and X-PLOR using a monomeric cyclinA-CDK2 model from the orthorhombic form crystal structure. The molecular replacement search yielded two distinct solutions which corresponded to the same n.c.s.-related dimer observed in the orthorhombic crystal form. The molecular replacement model was refined by simulated annealing (X-PLOR). Successive rounds of rebuilding and refinement were followed by restrained temperature factor refinement and anisotropic temperature factor correction (X-PLOR). $2F_o - F_c$ and $F_o - F_c$ electron density maps in the hexagonal crystal form had clear electron density for the adenine ring, the sugar, and the α -phosphate group of ATP which was consistent with the MIR electron density observed with the orthorhombic crystal form. In the final stages, ATP and water molecules were added to the model. The model was then further refined by simulated annealing with X-PLOR, and least-squares refinement with TNT⁴³. The β - and γ -phosphate groups of the ATP and the glycine-rich loop of CDK2 (residues 11–16) that anchors the phosphate groups have poor electron density in the maps, and high temperature factors in the refined model (similar apparent flexibility in the glycine-rich loop and phosphate groups have been observed in other kinase structures¹⁷). Other regions with high temperature factors and weak electron density include the 20 C-terminal amino acids of cyclinA (after the second repeat), and residues 38–41 of CDK2. **Structure in the presence of magnesium.** Because magnesium interfered with crystal growth, we attempted to determine whether this was caused by magnesium altering the structure of the bound ATP or of the cyclinA-CDK2 complex. An orthorhombic form cyclinA-CDK2-ATP crystal was soaked in 4 mM MgCl₂ for 2 days (Native-Mg) without any effect on diffraction quality. The 2.5 Å refined structure of the cyclinA-CDK2-ATP-Mg complex indicates that there are no significant changes in the structure when magnesium is present. The position of the magnesium was verified using data from a cyclinA-CDK2-ATP crystal soaked in a samarium solution [Sm(OAc)₃-Derivative]. The electron-dense samarium atom was located unambiguously in the catalytic site with difference Patterson and difference Fourier methods; it is bound by Asp 145 and has a position similar to that of the activating magnesium atom in the PKA structure²².

* $R_{\text{sym}} = \sum_n \sum_i |I_{h_i} - I_n| / \sum_n \sum_i I_{h_i}$ for the intensity (I) of i observations of reflection h .

† MFID, mean isomorphous difference = $\sum_i |F_{\text{PH}} - F_{\text{P}}| / \sum_i F_{\text{PH}}$, where F_{PH} and F_{P} are the derivative and native structure factors, respectively.

‡ Phasing power = $[(F_{\text{H(C)}})^2 / (F_{\text{PH(C)}} - F_{\text{PH(C)}})^2]^{1/2}$.

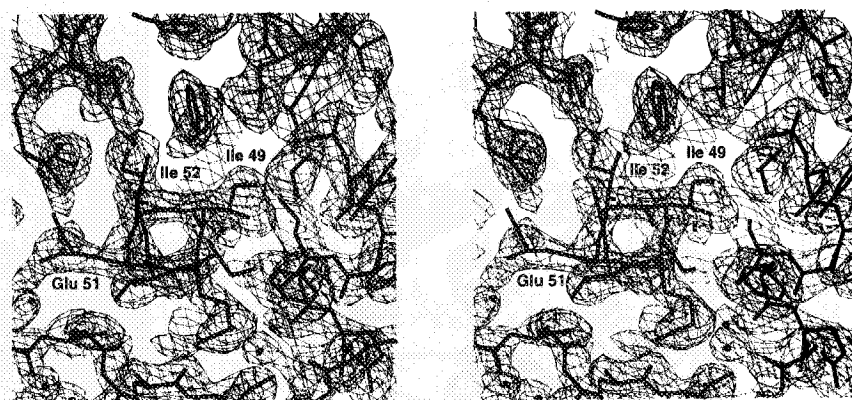
§ R-factor = $\sum |F_o - F_c| / \sum |F_o|$.

|| Root mean square deviations from ideal geometry, and r.m.s. variation in the B-factor of bonded atoms.

The $\alpha 1$ helix of CDK2, which contains the PSTAIRE sequence motif characteristic of the cyclin-dependent kinase family⁹ (Fig. 2a–c), is central to the interface. In cyclinA-bound CDK2, this helix rotates about its axis and moves several ångströms into the catalytic cleft, compared to free CDK2 (ref. 21). To make

space for it, the N-terminal sheet of CDK2 tilts away. The T-loop of CDK2, which contains the site phosphorylated in the fully active kinase (Thr 160 (ref. 26)), also interacts with cyclinA (Fig. 2a, b). Compared to free CDK2, this loop undergoes large conformational and positional changes which

FIG. 1 Electron density at the cyclinA-CDK2 interface in the vicinity of the PSTAIRE helix contoured at 1.2σ . The $(2|F_o| - |F_c|)$ Fourier synthesis was calculated at 2.3 Å resolution using phases calculated after omitting the interface residues shown, and subjecting the model to simulated annealing refinement (X-PLOR) from 2500K (interface residues within 12 Å of Ile 49 were omitted). Ile 49, Glu 51 and Ile 52 are labelled.



alter the positions of its residues by as much as 21 Å. CyclinA also contacts the N-terminal β -sheet and helices in the C-terminal lobe of CDK2.

Structure of cyclinA

The cyclinA fragment has a globular structure consisting of 12 α -helices. The molecule contains a structural repetition, having two sequential 90 amino acid domains with identical folds (residues 208–303 and 309–399, respectively; Fig. 3a, b). These folds consist of a right-handed three-helix bundle ($\alpha 1$, $\alpha 2$ and $\alpha 3$) with two additional helices ($\alpha 4$ and $\alpha 5$) packed against the bundle's side (the second repeat helices are named $\alpha 1'$ to $\alpha 5'$). The very similar structure of the two repeats—the Ca atoms of 78 of the 90 amino acids can be superimposed with an r.m.s. deviation of 1.7 Å (Fig. 3b)—was unexpected as the repeats are only 12% identical (Fig. 3c).

The repeats are connected by a linker of five amino acids, and pack loosely against each other across an interface that contains

three buried water molecules. They can be superimposed by a 160° rotation and an 11 Å translation about an axis approximately parallel to the helix bundle axis. In addition to the 10 helices in the two repeats, there is an additional α -helix (residues 179–190) N-terminal to the first repeat that packs against the second repeat, a helical extension to the second repeat (residues 408–412) and an extended region at the C terminus of the protein (residues 413–432).

The first repeat coincides with the cyclin box (residues 209–310; Fig. 3c). As expected from its sequence conservation, it is the key element at the cyclin-CDK2 interface, forming the binding site for the PSTAIRE helix and making contacts with the T-loop and the N-terminal β -sheet of CDK2. In general, the conservation of the different cyclinA elements across species parallels their role in CDK2 binding. For example, the first repeat is 78% similar to clam cyclinA²⁷; the N-terminal helix, which interacts with the C-terminal lobe of CDK2 and makes a large contribution to the buried surface area, is 56% similar;

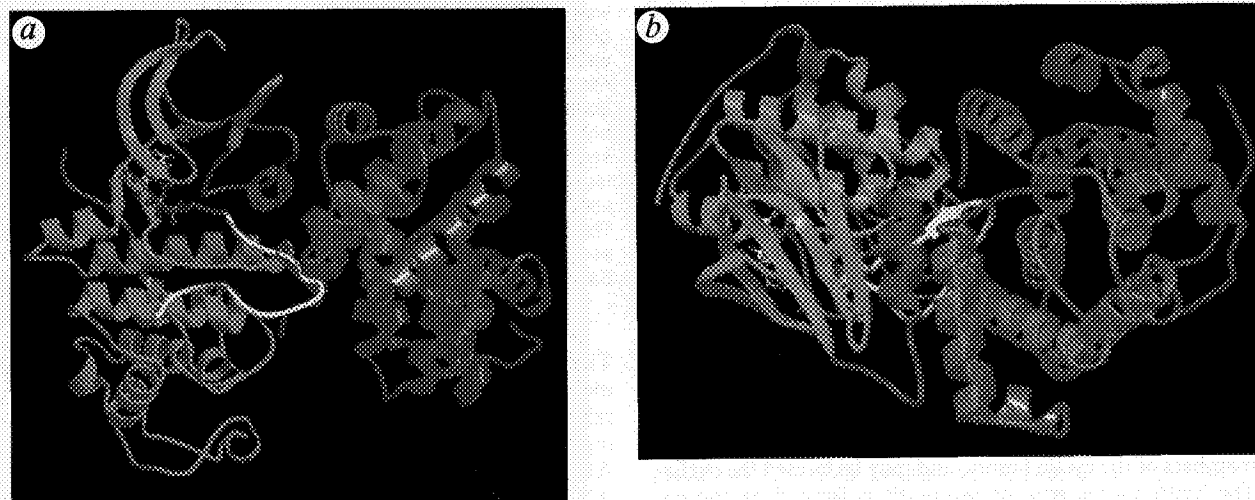
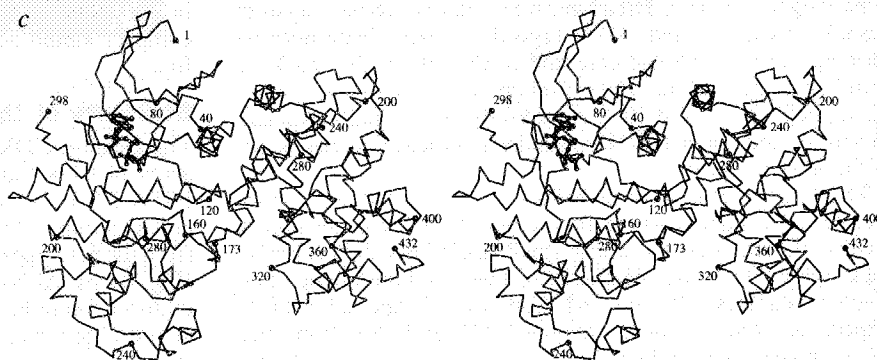


FIG. 2 a, Schematic drawing of the cyclinA-CDK2 complex. CyclinA is coloured magenta, CDK2 light blue; the ATP is shown as a ball and stick representation. Portions of CDK2 that undergo large conformational changes upon cyclinA binding are highlighted: the PSTAIRE region of CDK2 is red, the T-loop of CDK2 yellow. b, View of the complex looking down the vertical axis of a. The figures were done with the programs MOLSCRIPT⁴⁴ and RASTER3D⁴⁵. c, Stereo view of the Ca trace of the cyclinA-CDK2 complex in an orientation similar to that of Fig. 2a. Approximately every 40th residue is numbered and its Ca atom highlighted as a circle. The ATP is shown as a ball and stick representation.



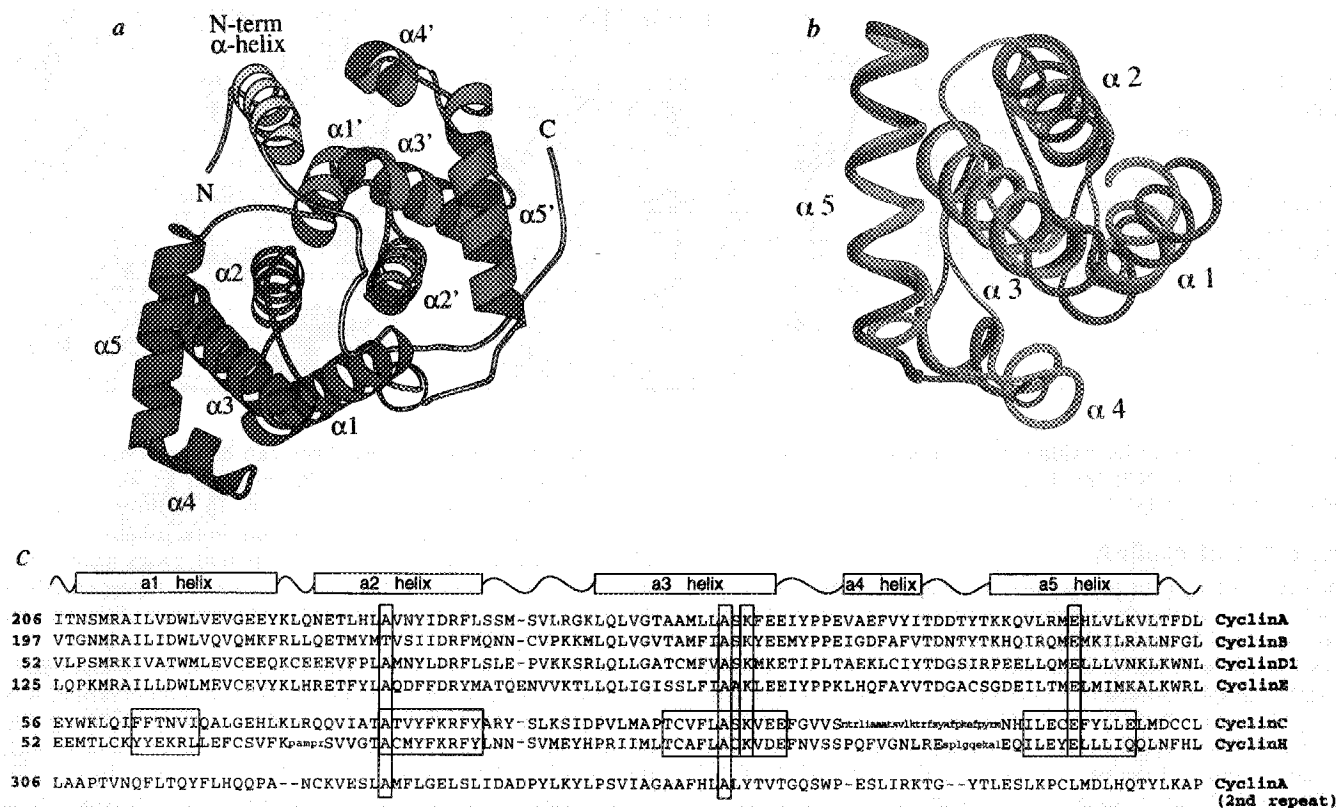


FIG. 3 *a*, View of the cyclinA structure (residues 173–432) highlighting the two structural repeats. The first repeat is coloured red, the second repeat green, the N- and C-terminal helices grey, and the individual helices are labelled. The two repeats are helices by a 160° rotation and an 11 Å translation about an axis perpendicular to the plane of the figure positioned approximately between helices $\alpha 2$ and $\alpha 2'$. The orientation of cyclinA is similar to that of Fig. 2*b*. *b*, The two repeats have very similar structures, and their Ca atoms can be superimposed with r.m.s. deviation of 1.7 Å (for 78 of the 90 amino acids). The backbone atoms for residues 211–303 of the first repeat (red) and residues 311–399 of the second repeat (green) are represented schematically. The different orientation of the $\alpha 1$ helix in the first repeat is correlated with a buried salt bridge between Arg 211 of the $\alpha 1$ helix and Asp 240 of the $\alpha 2$ helix. The salt bridge is buttressed by hydrogen bonds from the Arg 211 guanidinium group to the hydroxyl of Tyr 199 and to the backbone carbonyl groups of Leu 341 and Ile 342 (from the second repeat). The second repeat does not have an equivalent salt bridge, and its $\alpha 1'$ helix thus packs closer to the structure. *c*, The first cyclin

fold repeat of cyclinA coincides with the cyclin box, a region of approximately 100 amino acids conserved among members of the cyclin family. Sequence alignment showing the cyclin boxes of cyclinB (50% similarity to the cyclin box of cyclinA), cyclinD1 (40% similarity) and cyclinE (40% similarity) aligned with that of cyclinA¹⁵. Cyclins C²⁸ and H⁷ are more distantly related to cyclinA. The second cyclin fold repeat of cyclinA was aligned according to the structural alignment in *b*. The vertical boxes highlight the conserved alanine residues, which are likely to be characteristic of the cyclin fold, and also the lysine and glutamic acid residues that contact the backbone of CDK2 (the second cyclinA repeat does not contact CDK2 and thus it does not have the conserved lysine and glutamic acid residues). The boxes around the cyclin C²⁸ and H⁷ sequences indicate stretches of hydrophobic residues that match similar residues in the cyclin box cyclins. Insertions in the cyclin C and H sequences are in lower-case letters and probably replace the $\alpha 4$ helix. The secondary structure elements of cyclinA, indicated above the sequence, were defined according to criteria published by Kabsch and Sander⁴⁶.

and the second repeat, which plays only a minor role in the interface, is 48% similar.

Structure of the cyclin fold. The structural motif of five helices observed twice in the cyclinA fragment is probably common to other members of the cyclin family, and may be termed the cyclin fold. The hydrophobic core of the motif is formed by the $\alpha 3$ helix (Fig. 3*a, b*) whose central portion is surrounded by the remaining four helices. The $\alpha 1$ and $\alpha 2$ helices, which pack against the $\alpha 3$ helix at 43° and -47° , respectively, participate both in forming the hydrophobic core and in the inter-repeat packing with helices $\alpha 1'$ and $\alpha 2'$. Helices $\alpha 4$ and $\alpha 5$, which pack against the $\alpha 3$ helix at 39° and 105° , respectively, are partially exposed to solvent and contact CDK2. Similar interhelical angles occur in the second repeat.

The large angles between helices are associated with short interhelical distances where they cross. These crossing points involve alanine residues, whose small size allows the helices to pack tightly. The most significant of these packing interactions involves alanines 235 and 264 from the $\alpha 2$ and $\alpha 3$ helices, respectively (equivalent to alanines 333 and 363 from the second repeat), where the tight packing allows no substitutions.

This pair of residues is highly conserved among cyclin family members, including cyclins C and H which are only distantly related to the cyclin box cyclins^{7,28} (Fig. 3*c*). Additional crossing-point residues with small side chains include Gly 257, Ala 259 and Ala 260 from the $\alpha 3$ helix (equivalent to Ala 356, Ala 358 and Ala 359 from the second repeat). Although not as well conserved, these compact residues are also present in members of the cyclin family (Fig. 3*c*). This pattern of compact amino acids may thus be characteristic of the cyclin fold.

Structure of the cyclinA–CDK2 interface

The cyclinA–CDK2 interface is formed from an interlocking array of CDK2 and cyclinA elements (Fig. 4*a*), including the PSTAIRE helix, the T-loop, portions of the N-terminal sheet and C-terminal lobe of CDK2, and helices $\alpha 3$, $\alpha 4$ and $\alpha 5$ from the first repeat, as well as the N-terminal helix from cyclinA (Fig. 4*a, b*). Although the density of side chain contacts is not uniform, being highest around the PSTAIRE helix and lowest at the N-terminal sheet and C-terminal lobe, they result in a large buried surface area of $3,550 \text{ \AA}^2$ (Fig. 4*a, b*).

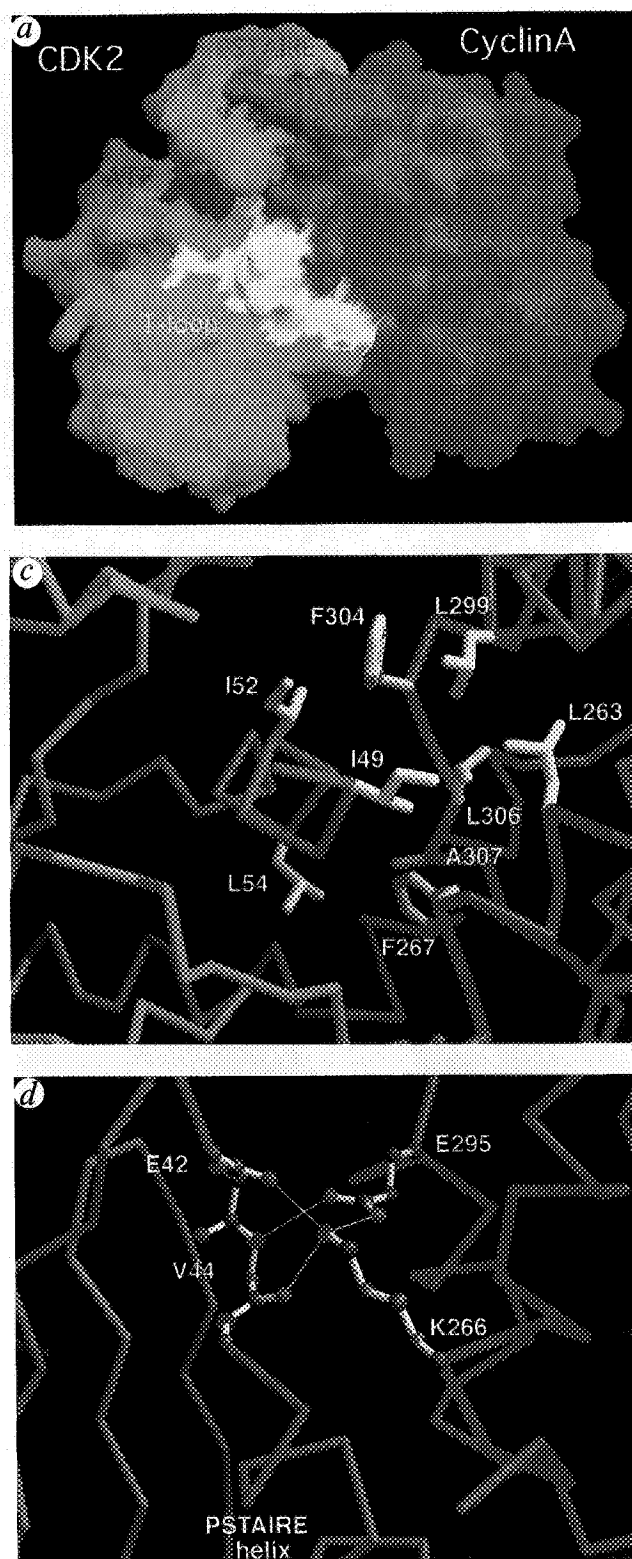
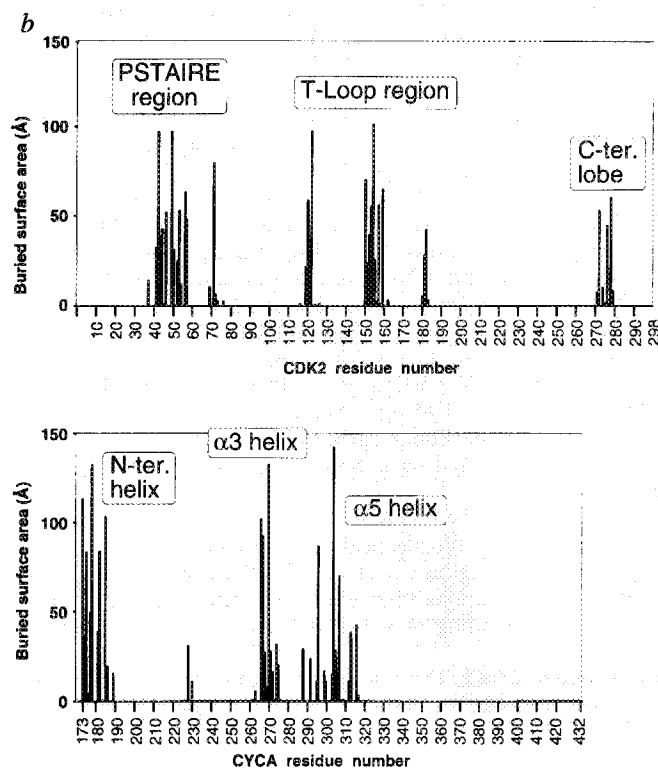


FIG. 4 *a*, The cyclinA-CDK2 interface consists of interdigitated cyclinA and CDK2 structural elements. Surface representation of the cyclinA (magenta)-CDK2 (cyan) complex highlighting the PSTAIRE region in red and the T-loop in yellow. The solvent-exposed ATP surface is shown

PSTAIRE region of CDK2. As shown in Fig. 2*a*, the cyclin box clamps onto and surrounds the middle part of the PSTAIRE helix (residues 46-56): the $\alpha 5$ helix lies parallel to the PSTAIRE helix on one side, and the C terminus of the $\alpha 3$ helix abuts the other side perpendicularly. This part of the PSTAIRE helix is



blue (orientation similar to that of Fig. 2*a*). The figure was done with the program GRASP⁴⁷. The surface area buried upon complex formation is substantially larger than most other heterologous protein-protein complexes whose structure is known, including the complex of enterotoxin B with a class II major histocompatibility molecule⁴⁸ (1540 \AA^2 buried), and antibody-protein complexes⁴⁹ (typically 1500 \AA^2 buried). *b*, Bar graph showing the differences in solvent accessibility⁵⁰ in cyclinA and CDK2 residues in the complex compared to the isolated subunits. The approximate locations of the structural elements discussed in the text are indicated. The cyclinA-CDK2 interface contains approximately 25 hydrophobic residues whose solvent accessibility is reduced substantially upon complex formation, and also contains 17 intermolecular hydrogen bonds between polar or charged amino acids. The following cyclinA-CDK2 interactions are not mentioned in the text: in the N-terminal β -sheet of CDK2, Val 69, His 71, Leu 76 and Leu 37 pack against His 296 and Phe 304 of cyclinA; in the C-terminal lobe, His 121 and the aliphatic portion of the Arg 122 side chain (both from the $\alpha 3$ helix of CDK2) make van der Waals contacts with Tyr 185 and Ile 182 of cyclinA, respectively, whereas the backbone amides of Ser 277 and Ala 278 (from the $\alpha 7$ helix of CDK2) donate a pair of hydrogen bonds to the hydroxyl of Tyr 178 of cyclinA. *c*, Close-up $C\alpha$ view of the interface showing the extensive hydrophobic side chain (yellow) interactions between the PSTAIRE helix of CDK2 and the cyclin box of cyclinA in an orientation and colouring similar to that of Fig. 2*a*. To make the buried hydrophobic interactions easier to see, only a section of the interface along the direction of the view axis is shown. Ile 49, Ile 52 and Leu 54 of CDK2, and Leu 263, Phe 267, Leu 299, Phe 304, Leu 306 and Ala 307 of cyclinA are labelled. In the structure of free CDK2, Ile 49 and Ile 52 of the PSTAIRE helix point away from the solvent and would be mostly inaccessible for cyclinA binding. *d*, Close up $C\alpha$ view of the network of side chain-backbone hydrogen-bond interactions in the loop preceding the PSTAIRE helix. To make the interactions easier to see, only the Lys 266 and Glu 295 side chains of cyclinA and the backbone groups of Glu 42-Val 44 of CDK2 are shown. Colours are as Fig. 2*a* except that atoms of interacting residues are red (oxygen), blue (nitrogen) and grey (carbon). The view is slightly rotated about the x- and y-axes with respect to that of Fig. 2*a*.

thus bound by an extended patch of hydrophobic interactions (Fig. 4*c*), whereas the N- and C-terminal regions are bound by networks of hydrogen bonds. Ile 49, in particular, fits tightly into a hydrophobic pocket lined with the side chains of Leu 263, Phe 267, Leu 299, Leu 306 and the aliphatic portion of Lys 266

from cyclinA (Fig. 4c). In addition, Ile 52 makes a van der Waals contact with Phe 304 of cyclinA and Leu 54 packs against Phe 267 and Ala 307 of cyclinA (Fig. 4c).

Immediately preceding the PSTAIRE helix, the backbone carbonyl groups of Glu 42 and Val 44 accept two hydrogen bonds from the Lys 266 side chain of cyclinA, and the backbone amide of Val 44 donates a hydrogen bond to the Glu 295 carboxylate of cyclinA (Fig. 4d). An additional hydrogen bond links the Lys 266 and Glu 295 side chains (Fig. 4d). The CDK2 loop conformation that allows this hydrogen-bond network relies on Gly 43, which adopts a backbone conformation ($\phi = 112^\circ$, $\psi = -150^\circ$) that other amino acids cannot adopt. The critical residues in this interaction, Lys 266 and Glu 295 of cyclinA, and Gly 43 of CDK2, are highly conserved.

In the C-terminal portion of the PSTAIRE helix, Lys 56 of CDK2 donates two hydrogen bonds to the Asp 305 side chain and the Thr 303 backbone carbonyl of cyclinA, and Glu 57 of CDK2 accepts a hydrogen bond from the Tyr 185 hydroxyl group of cyclinA.

The key role of the PSTAIRE helix at the interface is consistent with existing biochemical and genetic data. The exact sequence in this region correlates with the cyclin preference of CDKs⁹, and mutations there eliminate cyclin binding^{29,30}. Furthermore, the binding of anti-PSTAIRE antibodies is blocked by cyclins³¹.

The T-loop of CDK2. The T-loop region of CDK2 (residues 146–166), which blocks the entrance to the catalytic cleft in the free

kinase, is another major focus of cyclinA binding. In the complex, the N-terminal portion of the T-loop (residues 150–157) is bound by helices $\alpha 1$, $\alpha 2$ and $\alpha 3$ from the first repeat of cyclinA, as well as its N-terminal helix (Fig. 4a, b). Significant interactions include van der Waals contacts between Ala 151, Phe 152 and Tyr 159 of CDK2, and Phe 267, Ile 182 and Ile 270 of cyclinA, respectively. Hydrogen bonds also link the Arg 150 guanidinium group of CDK2 to the Glu 269 and Ile 270 backbone carbonyl groups of cyclinA and the side chains of Arg 157 (CDK2) and Gln 228 (cyclinA). CyclinA binding induces large conformational and positional changes in the T-loop, significantly relieving the blockade of the catalytic cleft observed in free CDK2.

N-terminal sheet and C-terminal lobe of CDK2. Interactions between the N-terminal β -sheet of CDK2 and the $\alpha 5$ helix of cyclinA are predominantly hydrophobic, whereas those between the C-terminal lobe of CDK2 and the N-terminal helix of cyclinA are also polar (Fig. 4a, b). Although these interactions are not as extensive as those of the PSTAIRE helix, they effectively exclude solvent and thus substantially extend the area of buried interface (Fig. 4a, b), presumably stabilizing the complex.

Conformational changes in CDK2

CyclinA alters the conformation of CDK2's PSTAIRE region and T-loop, and the relative orientation of its N- and C-terminal lobes. The C-terminal lobe, with the exception of the T-loop, is

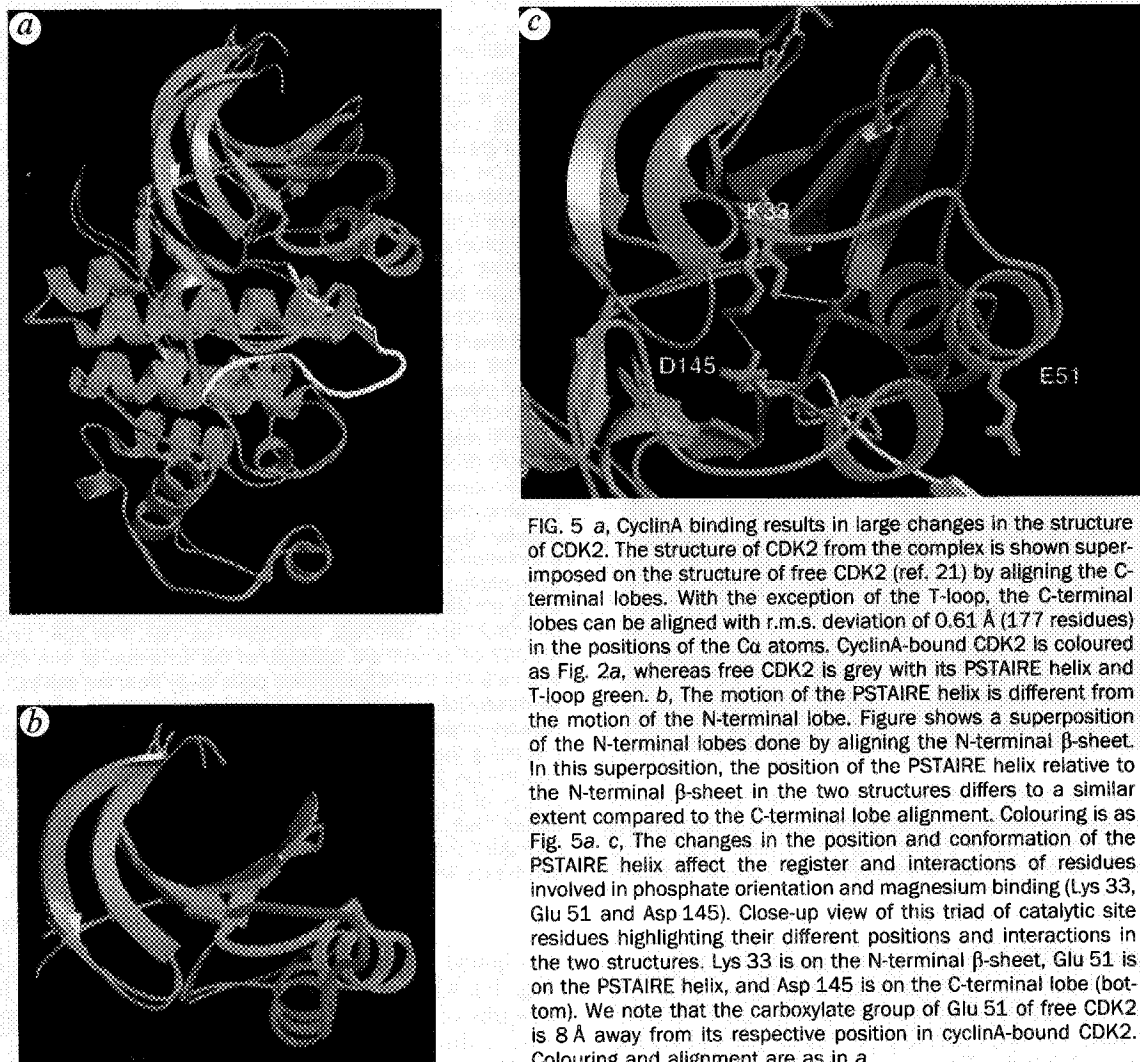


FIG. 5 a, CyclinA binding results in large changes in the structure of CDK2. The structure of CDK2 from the complex is shown superimposed on the structure of free CDK2 (ref. 21) by aligning the C-terminal lobes. With the exception of the T-loop, the C-terminal lobes can be aligned with r.m.s. deviation of 0.61 Å (177 residues) in the positions of the C_{α} atoms. CyclinA-bound CDK2 is coloured as Fig. 2a, whereas free CDK2 is grey with its PSTAIRE helix and T-loop green. b, The motion of the PSTAIRE helix is different from the motion of the N-terminal lobe. Figure shows a superposition of the N-terminal lobes done by aligning the N-terminal β -sheet. In this superposition, the position of the PSTAIRE helix relative to the N-terminal β -sheet in the two structures differs to a similar extent compared to the C-terminal lobe alignment. Colouring is as Fig. 5a. c, The changes in the position and conformation of the PSTAIRE helix affect the register and interactions of residues involved in phosphate orientation and magnesium binding (Lys 33, Glu 51 and Asp 145). Close-up view of this triad of catalytic site residues highlighting their different positions and interactions in the two structures. Lys 33 is on the N-terminal β -sheet, Glu 51 is on the PSTAIRE helix, and Asp 145 is on the C-terminal lobe (bottom). We note that the carboxylate group of Glu 51 of free CDK2 is 8 Å away from its respective position in cyclinA-bound CDK2. Colouring and alignment are as in a.

not significantly affected, and can be superimposed on that of free CDK2 with a 0.61-Å r.m.s. deviation in the C α positions (Fig. 5a). The C-terminal lobe will thus serve as a frame of reference in discussing the changes in CDK2.

Changes in the PSTAIRE region. The PSTAIRE helix starts with a helical hydrogen bond from the conserved Pro 45. On binding cyclinA, extensive hydrogen bonding (Fig. 4c) induces a conformational change in the loop immediately preceding the PSTAIRE helix (Fig. 5a, b), moving the Pro 45 starting residue. This is associated with a translation of the helix into the catalytic cleft towards the ATP and a rotation of roughly 90° about its helical axis, so that the backbone atoms in the helix are as much as 8.5 Å away from their counterparts in free CDK2 (Fig. 5a, b). The rotation changes the relative 'phase' of the helices in the two structures by approximately one residue. Towards the C terminus of the helix, the differences become smaller and the structures converge, as the C terminus of the helix is overwound and has a 3₁₀-like conformation in free CDK2.

The altered position and orientation of the PSTAIRE helix are associated with dramatic changes in its packing against the rest of CDK2. In free CDK2, packing is only loose, and the helix is apparently positioned to facilitate the conformational change accompanying cyclinA binding. Only two CDK2 residues make significant packing contacts: Ala 48 against the α L12 helix; and Ile 52 against the N-terminal lobe.

In cyclinA-bound CDK2, however, packing is much tighter, owing to (1) the lateral translation and the rotation of the PSTAIRE helix, and (2) the melting of the α L12 helix at the

beginning of the T-loop which prevents motion of the PSTAIRE helix in free CDK2. In the complex, the repositioned Ala 48 and Ile 52 pack extensively with Ile 35, Val 69, Leu 76 and Leu 78 in the N-terminal lobe. Furthermore, Leu 54, which in free CDK2 pointed out into solution, now points towards the C-terminal lobe and packs with Val 123 and Ala 151, while Leu 55, which was pointing into a water-filled internal cavity, now packs against Phe 80 and Phe 146.

The significance of this movement is that it brings the side chain of Glu 51, which belongs to a triad of catalytic site residues conserved in all eukaryotic kinases¹⁶, into the catalytic site. This triad (Lys 33, Glu 51 and Asp 145) is involved in ATP phosphate orientation and magnesium coordination, and is thought to be critical for catalysis³². In cyclinA-bound CDK2, Glu 51 lies in the catalytic cleft and makes a salt bridge with Lys 33, one of the residues that anchors the α and β phosphate groups of ATP, whereas Asp 145 binds the magnesium atom (Fig. 5c). These interactions are essentially identical to those observed in the catalytically active PKA structure²². In free CDK2, however, Glu 51 is outside the catalytic cleft and is mostly exposed to solvent. Its carboxylate group lies 8 Å from its position in cyclinA-bound CDK2, and cannot therefore form a salt bridge with Lys 33 (Fig. 5c). Instead, Lys 33 makes a salt bridge with Asp 145 (ref. 21), resulting in these residues adopting conformations and functions that differ from those observed in cyclinA-bound CDK2 and in PKA (Fig. 5c). This misalignment of active site residues probably plays a large part in the catalytic inactivity of free CDK2 (ref. 16).

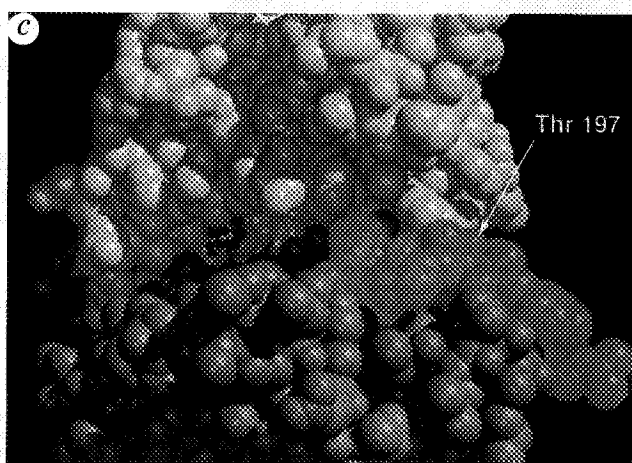
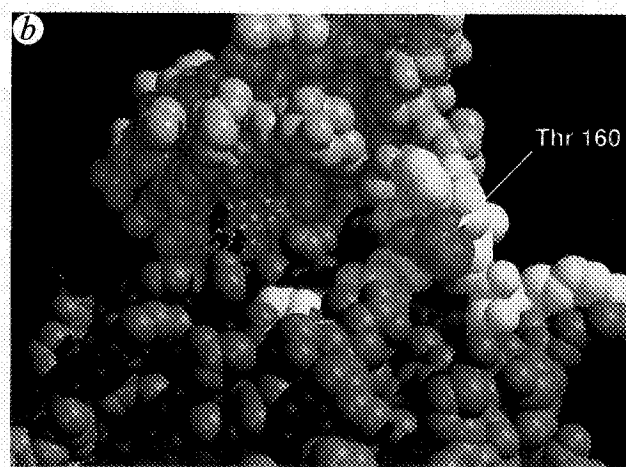
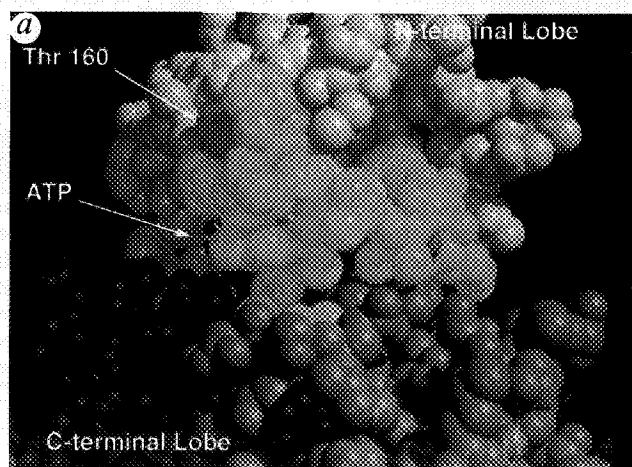


FIG. 6 a, CPK model highlighting the T-loop position relative to the ATP in the structure of free CDK2 (ref. 21). The C-terminal lobe is coloured dark grey, the N-terminal lobe light grey, the T-loop green and the Thr 160 phosphorylation site red. The ATP is mostly buried behind the

T-loop in this orientation. This conformation of the T-loop is presumed to block access of the protein substrate to the catalytic site²¹. b, CPK model highlighting the T-loop in the structure of cyclinA-bound CDK2. The colouring is as a, except that the T-loop is yellow (the structure was aligned on that of free CDK2 by superimposing the C-terminal lobes). The conformational change in the T-loop significantly relieves the blockade of the catalytic site by making the γ -phosphate of ATP fully accessible to the protein substrate. The change in the T-loop also exposes the Thr 160 side chain (red), making it a better substrate for phosphorylation. c, CPK model highlighting the catalytic site in the structure of the PKA (ref. 22). The region corresponding to the T-loop is shown blue, and the Thr 197 phosphorylation site red (the structure was aligned on that of free CDK2 by superimposing the C-terminal lobes). In cyclinA-bound CDK2 (b) and PKA (c), part of the loop is to the right and back side of the cleft and is thus not visible in this view. The conformational changes the T-loop undergoes upon binding to cyclinA make it resemble closely the respective region of PKA. With the exception of three residues at the Thr 160 phosphorylation site of cyclinA-bound CDK2, the T-loop (residues 146–166) can be superimposed on the equivalent region of PKA (residues 185–202) with r.m.s. deviation of 1.65 Å in the positions of their C α atoms. It is only in the immediate vicinity of the phosphorylation site that the two loops differ significantly where the C α atom of Thr 160 is 5 Å away from the C α atom of Thr 197, the equivalent residue in PKA.

Changes in the T-loop. In free CDK2, the Gly 147–Gly 153 region of the T-loop forms the α L12 helix, packing with the PSTAIRE helix and the N-terminal lobe (Fig. 5a). In cyclinA-bound CDK2, the α L12 helix melts, allowing the region instead to form a reverse turn (residues 146–149), followed by a β -sheet (residues 150–152) with the β 6 strand (residues 122–124) of the C-terminal lobe (Fig. 5a; a similar β -sheet occurs in the catalytically active PKA structure). The change also leads to new packing interactions with the repositioned PSTAIRE helix and with cyclinA (Arg 150, Ala 151 and Phe 152 interact with cyclinA as discussed earlier).

This change has a twofold significance. First, the α L12 helix prevents the PSTAIRE helix from moving into the catalytic cleft in free CDK2, and its melting on binding cyclinA enables the PSTAIRE helix to move. Second, the β -sheet that replaces the α L12 helix directs the T-loop away from the entrance of the catalytic cleft. At the end of the β -sheet, the T-loop is already 15 Å away from its position in free CDK2.

Beyond the α L12 region, the T-loop in free CDK2 (residues 154–164) criss-crosses the entrance of the catalytic cleft, rendering the ATP inaccessible to the protein substrate (Fig. 6a). In cyclinA-bound CDK2, this region is 12–21 Å from its position in free CDK2, well away from the entrance of the catalytic cleft and close to cyclinA (Fig. 6b; Arg 157 and Tyr 159 make additional contacts with cyclinA, as discussed earlier). The cyclinA-induced detour ends at the 164–166 region, by the end of which the Ca atoms in the bound and free forms are within 0.5 Å of each other. This detour substantially relieves the steric hindrance at the entrance to the catalytic cleft (Fig. 6a, b) and exposes the Thr 160 hydroxyl group phosphorylated by CAK, which in free CDK2 is buried in the catalytic cleft²¹ (Fig. 6a, b).

Comparison of the Thr 160 phosphorylation site with that of PKA. The conformational and positional changes induced by cyclinA in the T-loop leave it closely resembling the respective region of PKA²² (Fig. 6b, c). In cyclinA-bound CDK2, however, the Thr 160 side chain is unphosphorylated and points out into solution (Fig. 6b), whereas in PKA the equivalent residue (Thr 197) is phosphorylated, and its side chain is held close to the structure by multiple salt bridges between the phosphate group and three basic side chains (Fig. 6c). In the PKA-substrate complex²², this region forms part of the binding pocket for the hydrophobic substrate residue immediately following the phosphate acceptor, and its different conformation in the

unphosphorylated cyclinA-bound CDK2 may explain why the latter is only partially active.

When CDK2 is phosphorylated, the Thr 160 region may adopt a conformation similar to that of PKA, as cyclinA-bound CDK2 contains a cationic pocket that might bind the Thr 160 phosphate group in a manner analogous to that of PKA. The pocket contains the side chains of Arg 50, Arg 126 and Arg 150, which bind the carboxylate of Glu 162 in the unphosphorylated complex.

Change in the relative orientation of the N- and C-terminal lobes of CDK2. Apart from the PSTAIRE region, the isolated N-terminal lobe is not significantly altered by cyclin binding (Fig. 5b), but it moves relative to the C-terminal lobe, tilting away from the PSTAIRE helix and the entrance of the catalytic cleft so as to open the cleft (Fig. 5a). The overall rotation is about 14°, pivoting about a hinge region behind the cleft.

This movement makes space for the PSTAIRE helix to move into the catalytic cleft, but is otherwise unconnected with the motion of the PSTAIRE helix (Fig. 5b). The N-terminal lobe movement is also coupled to the changes the T-loop undergoes. In free CDK2, the T-loop criss-crosses the entrance to the catalytic cleft and interacts with the N-terminal β -sheet. On binding cyclinA, however, the N-terminal lobe's movement would not allow this interaction even if the T-loop did not move towards cyclinA. Finally, the N-terminal lobe movement also brings the side chain of Tyr 15, whose phosphorylation is thought to inhibit the kinase³³, deeper into the catalytic cleft. In the complex, the Tyr 15 side chain is within hydrogen-bonding distance of the Glu 51 carboxylate, and its phosphorylation may affect the positions of catalytic site residues and the ATP phosphates through steric hindrance and electrostatic repulsion.

Conclusion

The crystal structure of the cyclinA-CDK2 complex offers a general model for cyclin binding and CDK activation. Intimate interactions between the PSTAIRE region and the cyclin box form the centrepiece of the cyclin-CDK interface, and are likely to be key determinants of cyclin-CDK specificity. The activation of the kinase results from a conformational change in the PSTAIRE helix that realigns active site residues, together with a large motion of the T-loop that relieves the blockade of the catalytic cleft. The cyclin-T-loop interactions also expose Thr 160, making it a better substrate for phosphorylation by CAK and setting the stage for the full activation of the kinase. □

Received 24 May; accepted 29 June 1995.

- Morgan, D. O. *Nature* **374**, 131–134 (1995).
- Pines, J. *Biochem. Soc. Trans.* **21**, 921–925 (1993).
- Sherr, C. J. *Cell* **79**, 551–555 (1994).
- Heichman, K. A. & Roberts, J. M. *Cell* **79**, 557–562 (1994).
- Sobczak-Thepot, J. et al. *Exp. Cell Res.* **208**, 43–48 (1993).
- King, R. W., Jackson, P. K. & Kirschner, M. W. *Cell* **79**, 563–571 (1994).
- Fisher, R. P. & Morgan, D. O. *Cell* **78**, 713–724 (1994).
- Connell-Crowley, L., Solomon, M. J., Wei, N. & Harper, J. W. *Molec. Biol. Cell* **4**, 79–92 (1993).
- Pines, J. *Semin. Cancer Biol.* **5**, 305–313 (1994).
- Ewen, M. E. et al. *Cell* **73**, 487–497 (1993).
- Peepker, D. S. et al. *EMBO J.* **12**, 1947–1954 (1993).
- Dynlacht, B. D., Flores, O., Lees, J. A. & Harlow, E. *Genes Dev.* **8**, 1772–1786 (1994).
- Nigg, E. A. *Curr. Opin. Cell Biol.* **5**, 187–193 (1993).
- Langgan, T. A. et al. *Molec. Cell Biol.* **9**, 3860–3868 (1989).
- Hadwiger, J. A., Wittenberg, C., Richardson, H. E., De Barros Lopes, M. & Reed, S. I. *Proc. natn. Acad. Sci. U.S.A.* **86**, 6255–6259 (1989).
- Taylor, S. S. & Radzio-Andzelm, E. *Structure* **2**, 345–355 (1994).
- Zhang, F., Strand, A., Robbins, D., Cobb, M. H. & Goldsmith, E. J. *Nature* **387**, 704–711 (1994).
- Hubbard, S. R., Wei, L., Ellis, L. & Hendrickson, W. A. *Nature* **372**, 746–754 (1994).
- Hu, S. H. et al. *Nature* **369**, 581–584 (1994).
- Xu, R. M., Carmel, G., Sweet, R. M., Kuret, J. & Cheng, X. *EMBO J.* **14**, 1015–1023 (1995).
- De Bondt, H. L. et al. *Nature* **363**, 595–602 (1993).
- Knighton, D. R. et al. *Science* **263**, 407–413 (1991).
- Kobayashi, H. et al. *Molec. Biol. Cell* **3**, 1279–1294 (1992).
- Lees, E. M. & Harlow, E. *Molec. Cell Biol.* **13**, 1194–1201 (1993).
- Polyak, K. et al. *Cell* **75**, 59–66 (1994).
- Desai, D., Gu, Y. & Morgan, D. O. *Molec. Biol. Cell* **3**, 571–582 (1992).
- Standart, N., Dale, M., Stewart, E. & Hunt, T. *Genes Dev.* **4**, 1257–1268 (1990).
- Lew, D. J., Dulic, V. & Reed, S. I. *Cell* **60**, 1197–1206 (1991).
- Ducommun, B. et al. *EMBO J.* **10**, 3311–3319 (1991).
- Marcote, M. J. et al. *Molec. Cell Biol.* **13**, 5122–5131 (1993).
- Pines, J. & Hunter, T. *Cell* **58**, 833–846 (1989).
- Zheng, J. et al. *Biochemistry* **32**, 2154–2161 (1993).
- Solomon, M. J. *Curr. Opin. Cell Biol.* **5**, 180–186 (1993).
- Rosenblatt, J., De Bondt, H., Jancarik, J., Morgan, D. O. & Kim, S. J. *molec. Biol.* **230**, 1317–1319 (1993).
- SERC (UK) Collaborative Computing Project No. 4 (Daresbury Laboratory, Warrington, 1979).
- Furey, W. & Swaminathan, S. *Am. Crystallogr. Ass. Meet. Abstr. Ser.* **2**, 18, 73 (1990).
- Jones, T. A. in *Molecular Replacement* (ed. Dodson, E. J.) 91–105 (SERC, Daresbury, 1992).
- Jones, T. A., Zou, J.-Y. & Cowan, S. W. *Acta Crystallogr.* **A47**, 110 (1991).
- Sack, J. S. *J. molec. Graphics* **6**, 224 (1988).
- Brunger, A. T. *X-PLOR, a system for crystallography and NMR, Version 3.0* (Yale Univ. Press, New Haven, CT, 1991).
- Fitzgerald, P. M. D. *J. appl. Crystallogr.* **21**, 273 (1988).
- Fujinaga, M. & Read, R. J. *J. appl. Crystallogr.* **20**, 273 (1987).
- Tonrud, D. E., Ten Eyck, L. F. & Matthews, B. W. *Acta Crystallogr.* **A43**, 489 (1987).
- Kraulis, P. J. *J. appl. Crystallogr.* **24**, 946–950 (1991).
- Merrit, E. A. & Murphy, M. E. *Acta Crystallogr.* **50B**, 869–873 (1994).
- Kabsch, W. & Sander, C. *Biopolymers* **22**, 2577–2637 (1983).
- Nicholls, A., Sharp, K. A. & Honig, B. *Proteins: Structure, Function and Genetics*, **11**, 281–296 (1991).
- Jardetzky, T. S. et al. *Nature* **366**, 711–718 (1994).
- Davies, D. R., Padlan, E. A. & Sheriff, S. A. *Rev. Biochem.* **59**, 439–473 (1990).
- Lee, B. & Richards, F. M. *J. molec. Biol.* **55**, 379–400 (1971).

ACKNOWLEDGEMENTS. P.D.J. and A.A.R. contributed equally to this work. We thank B. Chait and U. Minza for the mass spectroscopic analysis; S. Geromanos for N-terminal sequence analysis; Z. O. Pan for the CDK activating kinase preparation; D. O. Morgan for the CDK2-expressing baculovirus vector; S. H. Kim for the coordinates of the free CDK2 crystal structure; E. Stebbins for help with data collection; the staff of the Cornell High Energy Synchrotron Source MacChess for help with data collection; and R. Kenny for administrative help. This work was supported by the NIH, the Pew Charitable Trusts, the Dewitt Wallace Foundation, and the Samuel and May Rudin Foundation. Coordinates will be deposited with the Brookhaven Protein Data Bank.